SPACE SCIENCES

In situ detection of water on the Moon by the Chang'E-5 lander

Honglei Lin[1]†, Shuai Li[2]†, Rui Xu[3]†, Yang Liu[4,5]*, Xing Wu[4], Wei Yang[1], Yong Wei[1], Yangting Lin[1]*, Zhiping He[3]*, Hejiu Hui[5,6], Huaiyu He[1], Sen Hu[1], Chi Zhang[1], Chunlai Li[3], Gang Lv[3], Liyin Yuan[3], Yongliao Zou[4], Chi Wang[4]

We report analysis results of the reflectance spectra (0.48 to 3.2 μm) acquired by the Chang'E-5 lander, which provides vital context of the returned samples from the Northern Oceanus Procellarum of the Moon. We estimate up to 120 parts per million (ppm) of water (OH + H$_2$O) in the lunar regolith, which is mostly attributed to solar wind implantation. A light-colored and surface-pitted rock (named as CE5-Rock) is evident near the lander. The reflectance spectra suggest that CE5-Rock could be transported from an older basalt unit. CE5-Rock exhibits a stronger absorption, near 2.85 μm, than the surrounding regolith, with estimation of ~180 ppm of water if the model for estimating water content of regolith is applicable to rock samples, which may suggest an additional source from the lunar interior. The low water content of the regolith may suggest the degassing of mantle reservoir beneath the Chang'E-5 landing site.

INTRODUCTION

The Chang'E-5 spacecraft landed in the Northern Oceanus Procellarum basin (43.06°N, 51.92°W) on the Moon on 1 December 2020 and successfully returned 1.731-kg samples on 17 December 2020 (Fig. 1A). This is the first lunar sample return mission since the Soviet Union's Luna 24 mission in 1976. The landing area is located in the Procellarum KREEP (potassium, rare earth elements, and phosphorus) Terrane (PKT) (1), and the mare basalt at the landing site is suggested to be very young (~2.0 billion years), younger than all the known lunar basalts (2–6). The lander is equipped with a Panoramic Camera (PCAM), a Lunar Mineralogical Spectrometer (LMS), and a Lunar Penetrating Radar to explore the surface topography, the mineral compositions, and the subsurface structure of the landing area. In this study, we report a detailed spectroscopic study using the data acquired by the LMS onboard the Chang'E-5 lander.

The LMS operated in multispectral and hyperspectral modes. The multispectral mode aimed to obtain the context images of the surface around the landing site (Fig. 1B). The hyperspectral mode covered the spectral range from 0.48 to 3.2 μm with a spectral interval of 5 nm (7), which allows measurement of the mineral compositions and the total water content (OH + H$_2$O) of lunar materials at the landing site. Reflectance spectra of the regolith and a rock around the sampling site were acquired by the LMS (Fig. 1B). The data were first converted to radiance and calibrated, using the preflight calibration database measured with integrating spheres and blackbody in the vacuum chamber by the engineering team. The in-flight calibration was also performed to a radiance data, using an aluminum-based diffuse reflectance standard and a customized InfraGold standard onboard the lander. The in-flight calibrated radiance was converted into reflectance plus thermal component (fig. S1) and then thermally and photometrically corrected, using a semiempirical model and Hapke model (8, 9), respectively (see Materials and Methods).

Multiple geologic units were mapped and investigated near the Chang'E-5 landing site in previous studies (2, 4). The northwestern mare unit was dated as Imbrian age from crater counting and exhibits low TiO$_2$ contents [~1.3 weight % (wt %)] (fig. S3) (10, 11). The landing region is within the young Eratosthenian mare basalt unit and contains a moderate amount of TiO$_2$ (~5.7 wt %) estimated using the Kaguya Multiband Imager data (10, 11). The mean thickness of the young mare basalts at the landing site was estimated to be ~51 m (12). An underlying unit exhibits similar features as the low-Ti mare basalt unit in the northwestern mare region of the landing site (3). As revealed by the PCAM images (Fig. 1A), the landing area is covered mostly by dark regolith with only a few small pieces of brighter rocks sporadically on the surface (less than 50 cm in size) (Fig. 1). There are abundant dark spots on the surface of these brighter rocks. If these are vesicles, then strong degassing is suggested during the emplacement of the host rock. Hyperspectral reflectance data of the rock D11 (named as "CE5-Rock" hereafter; Fig. 1B) were collected by the LMS. The reflectance data of the regolith at several spots nearby CE5-Rock were also acquired. The thermally and photometrically corrected LMS reflectance spectra at eight spots nearby the lander (Fig. 1) are shown in Fig. 2 and fig. S1. These data were processed to assess the mineralogy and water contents of the surface materials at the Chang'E-5 sampling site. Our results provide the field geological context for the returned samples and establish the relationship between the in situ measurements and the laboratory analyses of the returned samples.

RESULTS AND DISCUSSION

The spectrum of CE5-Rock exhibits a strong absorption at 2.85 μm because of the presence of OH/H$_2$O (Fig. 2). By contrast, most of the lunar regolith at the landing site exhibit no/weak absorptions at
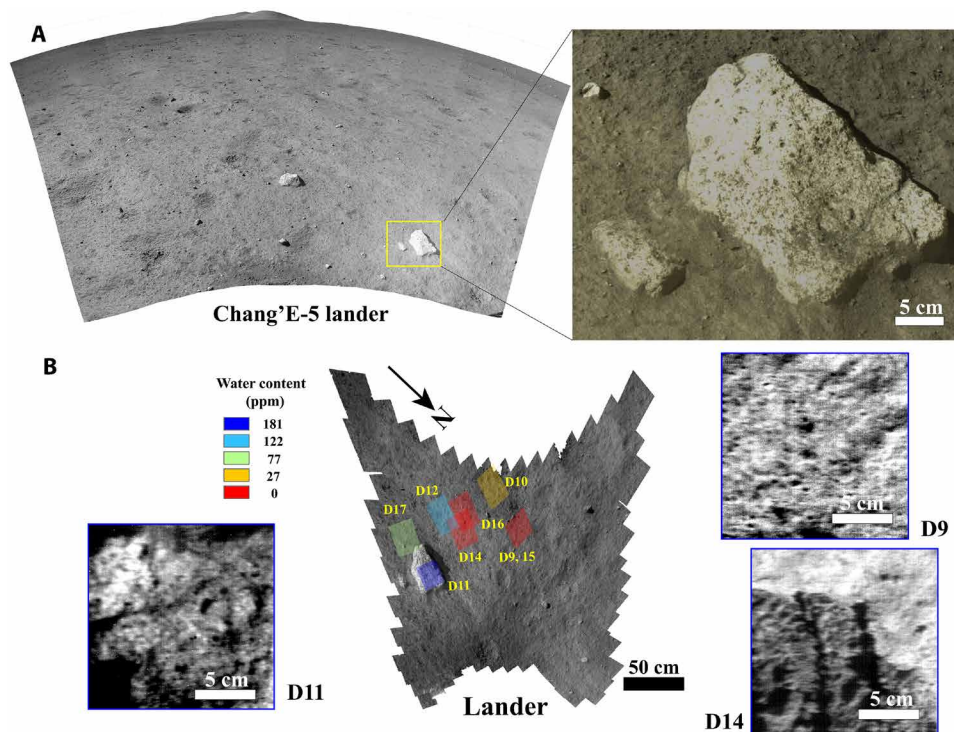
Fig. 1. The context images at the Chang'E-5 landing site captured by the PCAM and LMS. (**A**) The PCAM image of the sampling site. The right panel shows the enlarged image of the rock from which the reflectance spectra were collected by the LMS. (**B**) The image (0.4 to 1.0 mm per pixel) at 900 nm acquired by the multispectral mode of the LMS at the sampling site. The colored rectangles represent the exact spots on the surface where the hyperspectral data from 0.48 to 3.2 μm were acquired. The viewing geometry of each observation is shown in table S1. LMS hyperspectral mode images (~0.6 mm per pixel) at D9, D11, and D14 are shown as examples of the regolith textures in the LMS FOV. Similar texture images at other spots can be found in fig. S2. The water contents of each spot are estimated from the absorption strength near 3 μm using the method in (*9*) after thermal removal with the model in (*8*).

~2.85 μm, similar to the Moon Mineralogy Mapper (M^3) spectra over the region (Fig. 2). The 2.85-μm absorption band in the rock spectrum is about twice stronger than that in the regolith spectra, as shown in both their original and the continuum-removed spectra (fig. S4), indicating potentially higher water content in the rock. The water content of each LMS target was estimated (Fig. 1B), on the basis of the absorption features near 3 μm in the thermally corrected spectra (*8*). The effective single-particle absorption thickness (ESPAT) at 2.85 μm was calculated for each of the LMS spectra to derive the water contents (see Materials and Methods). The laboratory studies on hydrous minerals revealed that the absolute water contents can be linearly correlated with the ESPAT values at 2.85 μm (*13*, *14*), and the linear coefficient varies with the particle size of lunar analogs (*9*, *14*). The uncertainty of the estimated water content from ESPAT is ~20% (*9*). We used the mean particle size of lunar regolith of 60 to 80 μm in our modeling, which is similar to the particle size of the regolith determined by mass at the six Apollo and Chang'E-5 landing sites (*15*, *16*). The derived water content of the regolith at the Chang'E-5 landing site varies from nearly undetectable [<~30 parts per million (ppm)] to around 120 ppm (Fig. 1B and table S2). The water contents are less than 30 ppm in most measured regolith spots except for D12 and D17 (Fig. 1), which may be due to the disturbance of the top layer of the more space-weathered/solar wind–implanted regolith (*17*) by the lander exhaust and the subsequent sampling process. The unsampled areas of D12 and D17 may have been shielded by the CE5-Rock from the lander exhaust (fig. S5) and thus retain the top space-weathered layer that contains higher water content. We predict
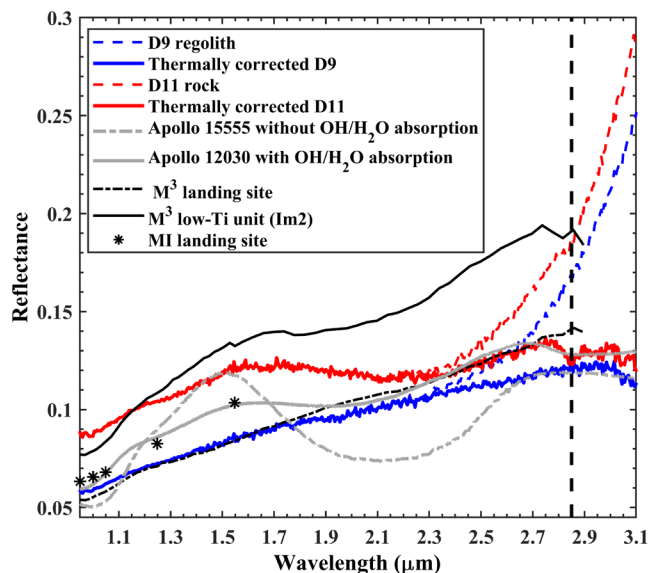

Fig. 2. Examples of thermally and photometrically corrected Chang'E-5 LMS reflectance spectra. The Moon Mineralogy Mapper (M^3) and Kaguya Multiband Imager (MI) spectra collected from regions nearby the landing site (fig. S3) are shown for comparison. The spectra [spectrum IDs in Reflectance Experiment Laboratory (RELAB): N2LS01 and LALR32] of Apollo samples are offset for clarity. All other LMS spectra are shown in fig. S1. The vertical black dashed line indicates the wavelength of 2.85 μm. Data below 0.95 μm and above 3.1 μm were removed from the LMS spectra to avoid artifacts near the two edges of the detectors.

that higher water content may be found in surface regolith than that from the subsurface of the returned borehole samples if the original stratigraphy is preserved. The estimated water contents of the regolith in the landing area are in agreement with those measured in the Apollo regolith samples (18) and the orbital observations (9, 19). Similar to the Apollo regolith samples (18, 20), water in the regolith at Chang'E-5 landing site likely originates mainly from solar wind implantation (18). To calculate the water content of CE5-Rock, two scenarios were considered in terms of the particle size. The reflectance near 3 µm of CE5-Rock is mostly from the top 1-mm layer (the optical depth of light near 3 µm), because most of the light that propagates beyond the optical depth (approximately in millimeters) cannot be reflected to the sensor. In this case, the derived water content is around 70 ppm (table S2), which is similar to that observed in the surrounding regolith. Thus, it is difficult to determine whether the water came from solar wind implantation or the rock itself derived originally from the lunar interior. Alternatively, the top surface of CE5-Rock may have been space-weathered to fine particles (e.g., 60 to 80 µm), and the derived water content is around 180 ppm, which is much higher than those of the surrounding regolith (Fig. 1B). The excess water signature in CE5-Rock may suggest extra sources of water in addition to solar wind implantation.

The spectral features of CE5-Rock suggest that it may be transported from a different geologic unit to the Chang'E-5 landing site. The mineral abundances and grain sizes of the regolith and CE5-Rock at the Chang'E-5 landing site were estimated from the reflectance spectra between 0.5 and 2.5 µm acquired by the LMS in conjunction with the Hapke spectral unmixing model (21, 22) (see Materials and Methods). The endmembers used in the unmixing model are listed in table S3. The modeling results show that the particle sizes are between ~50 and 80 µm for regolith and ~60 µm for CE5-Rock, verifying that the particle size range used to estimate the water content is effective (table S4). The derived mineral composition of the CE5-Rock from the unmixing model is distinct from that of the surrounding regolith (Fig. 3 and fig. S6), with more abundant plagioclase and less ilmenite (table S4). This is consistent with the lighter color of CE5-Rock. Thus, CE5-Rock could have been excavated and ejected

from beneath or the surrounding older low-Ti basalt (3, 4). Several fresh craters near the Chang'E-5 landing site are large enough to penetrate the top basalt unit (~50 m thick). This is consistent with the M³ spectra of the ejecta rims of these fresh craters (fig. S3). Alternatively, this rock may have been ejected from the adjacent older low-Ti mare basalt unit (fig. S3). It should be noted that the endmember viability can introduce some uncertainties on the retrieved mineral abundances, and applying unmixing model to non-particulate samples such as CE5-Rock is not well tested, which both need further study based on the returned samples in the laboratory.

CE5-Rock appears to be full of vesicles (Fig. 1), suggesting strong volatile degassing during emplacement. Our modeling results suggest that the surface of CE5-Rock is fine-grained in texture, which is also commonly found in rapidly cooled mare basalts of Apollo samples (23). If that is the case, then our estimation of water content at around 180 ppm based on an effective particle size of 60 to 80 µm is reasonable, which is at least 60 ppm higher than that of the surrounding regolith (Fig. 1B). The value of 60 ppm is notably higher than our model uncertainty of 36 ppm (20% of 180 ppm). The "excess" water detected in the CE5-Rock may originate from additional sources, such as remnant water within a rock derived originally from the lunar interior (19, 24–26). Thus, the magma source of CE5-Rock could be water rich (27). Notably, the older low-Ti mare basalt unit on the northwest of the sampling site where the CE5-Rock could have been transported also exhibits anomalously high water content that was attributed to a source from the lunar interior (28). However, it is noteworthy that our model for estimating water content from the visible–near infrared reflectance spectra was developed from powder samples, and it may bring larger uncertainties than 20% when applying to rock samples because of the substantial differences of optical properties between the former and latter. In addition, the estimated water content of CE5-Rock drops to ~70 ppm if we assume a larger effective particle size of CE5-Rock (1 mm), which is equivalent to that of the surrounding regolith and suggests no excess water in CE5-Rock. This case would likely be unrealistic given a rapid cooling implied by the possible vesicles. We thus suggest that CE5-Rock has more inherent water than other materials seen at
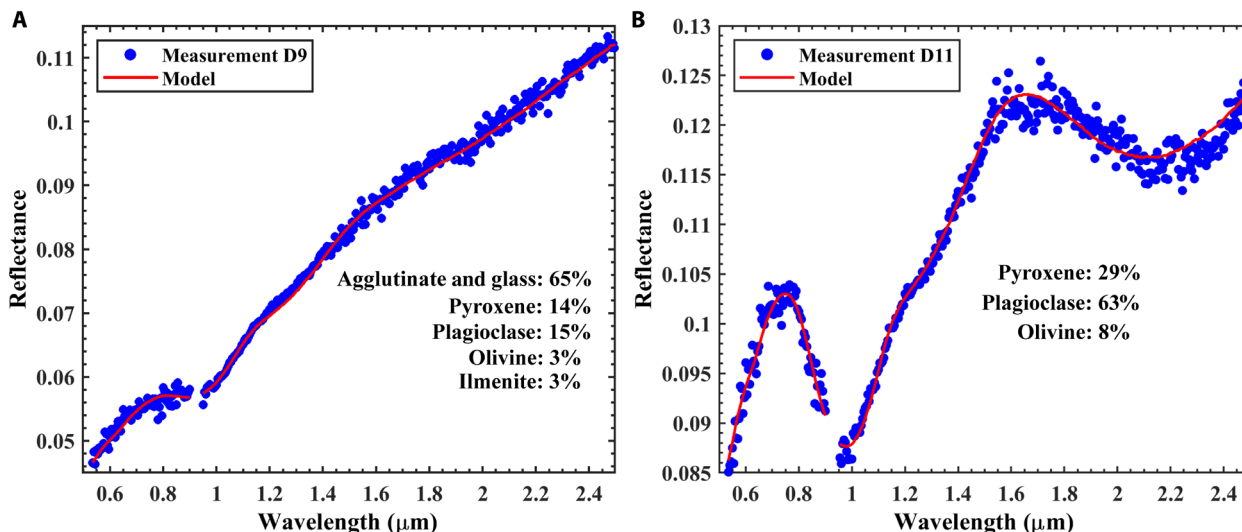

Fig. 3. The spectral modeling results of the LMS data acquired by the Chang'E-5 lander using Hapke's radiative transfer model. (**A**) An example spectrum of lunar regolith D9. (**B**) An example spectrum of CE5-Rock.

the site. A future revisit of the water content of CE5-Rock is necessary to nail down whether lunar interior water exists in CE5-Rock when a new model for estimating water content of rock samples will be available. Anyhow, the low water content of the regolith may suggest a dry mantle or substantial degassing at least beneath the Chang'E-5 landing area, which is consistent with the prolonged volcanic eruptions in the PKT region (*29*). It remains unclear whether our detected water is hydroxyl or molecular water because of the lack of full coverage of the whole 3-μm region between ~2.65 and 4 μm (*9*). Analyzing the water and other volatile contents as well as the speciation of hydroxyl and molecular water of lithic fragments of vesicular rocks in the returned samples is warranted in future studies.

MATERIALS AND METHODS
In situ spectra acquired by LMS onboard the Chang'E-5 lander
The LMS onboard the Chang'E-5 lander measured the spectra of lunar regolith and rocks at the height of ~1.4 m before returning samples. The LMS obtains spectra by covering the visible to infrared range (480 to 3200 nm) with 5-nm spectral-sampling interval. The detector of LMS in visible–near-infrared wavelengths can obtain the image with a spatial resolution of ~0.6 mm. The spectral resolutions of the LMS are 2.4 to 9.4 nm in the spectral range of 480 to 1450 nm and 7.6 to 24.9 nm in the 1400 to 3200 nm. The LMS used integrating spheres and blackbodies to calibrate spectral radiance in the laboratory and acquired radiance correction data in a vacuum tank. The uncertainty of the radiometric calibration is lower than 6% at most of the bands. The aluminum-based diffuse reflector plate and the customized InfraGold standard plate (LabSphere Inc.) are installed in the dustproof and calibration unit of the LMS. In-flight calibration was performed using the correction coefficient derived from the relationship between the measured radiance and theoretical radiance of the standard plate.

Thermal and photometric correction of LMS data
We followed an empirical model developed by Li and Milliken (*8*) to remove the thermal effects from the measured LMS spectra. This empirical model was developed on the basis of the laboratory reflectance spectra of Apollo and Luna samples with a wide range of compositions and maturity. The reflectance at a short wavelength of 1.55 μm and a long wavelength of 2.54 μm was selected to establish an empirical relationship because these two bands avoid the major absorptions of lunar materials. The data at 1.55 μm are not affected by thermal emission. The wavelength of 2.54 μm lies outside of the OH/H_2O absorption and may receive thermal contaminations under the lunar surface temperatures. The "true" radiance at 2.54 μm can be predicted using the empirical relationship, any excess radiance of the LMS measurements is attributed to thermal emissions, and temperatures can then be derived from the Planck function (*8*). The derived temperatures are used to remove thermal emissions from other spectral bands that may have also been contaminated by thermal emissions. This empirical model has been successfully applied to M^3 spectra (*9*, *19*), and similar procedures were also used to estimate the surface temperatures and remove thermal effects from in situ reflectance spectra at the Chang'E-4 landing site (*30*).

We used Hapke's model to perform the photometric correction for all LMS data after thermal removal in the previous step (*8*). A two-term Legendre polynomial was used to model the phase function

of lunar regolith, which is similar to those used in (*31*, *32*). The field of view (FOV) of the LMS is equivalent to that of laboratory spectrometers (e.g., approximately a few centimeters in size). Thus, the empirically derived two-term Legendre polynomial is applicable to the LMS experiments on the lunar surface. Previous laboratory studies using lunar analogs such as pyroxene, plagioclase, olivine, and ilmenite that typify the lunar surface show that a two-term Legendre polynomial is sufficient to represent how light intensity changes with phase angles. In this study, we adopted the coefficient *b* and *c* of the Legendre polynomial derived for lunar analogs in our photometric corrections of the LMS data.

Deriving mineral abundance from the reflectance spectra of lunar surface
The abundances of major minerals in the lunar regolith and rocks at the Chang'E-5 landing site are estimated from the reflectance spectra at 0.5 to 2.5 μm, acquired by LMS in conjunction with the Hapke spectral unmixing model (*21*). The dominant minerals on the lunar surface—including clinopyroxene, orthopyroxene, olivine, plagioclase, ilmenite, agglutinate, and volcanic glasses (table S3)—were chosen as the endmembers (*22*, *33*, *34*) in our spectral unmixing. The same implementation of Hapke's model was performed on Apollo samples in the Lunar Soil Characterization Consortium dataset (*34*). The residual of curve fitting (e.g., the ability to reproduce measured reflectance spectra) in spectral unmixing analyses is commonly used as an indicator for estimated endmember abundances (*35*).

Hapke's model describes the relationship between reflectance with single-scattering albedo (SSA), viewing geometry, and multiple-scattering function

$$r(i, e, g) = \frac{\omega_{ave}\mu_0}{4(\mu_0 + \mu)}\{[1 + B(g)]P(g) + H(\mu_0, \omega_{ave})H(\mu, \omega_{ave}) - 1\} \quad (1)$$

where, $r(i, e, \alpha)$ reflectance (radiance factor) and *i*, *e*, and *g* are incidence angle, emission angle, and phase angle, respectively. μ_0 and μ are cosines of *i* and *e*, respectively. $B(g)$ accounts for the opposition surge effect, $P(g)$ is the phase function, and *H* is the multiple-scattering function. The expressions and parameterizations of $B(\alpha)$, $P(g)$, and *H* are the same with those of (*22*). ω_{ave} is average SSA.

The SSA of each endmember is a function of the optical constants *n* and *k* and the optical path length <D>, as described in (*21*, *22*). We set <D> = 0.2D by assuming the irregular shape of particles (*36*). For considering the effects of space weathering to lunar surface, the submicroscopic metallic Fe (SMFe) was modeled to modify the absorption coefficient of each endmember

$$\alpha = \frac{4\pi n k}{\lambda} + \frac{36\pi z M_{Fe}\rho}{\lambda \rho_{Fe}} \quad (2)$$

$$z = \frac{n^3 n_{Fe} k_{Fe}}{(n_{Fe}^2 - k_{Fe}^2 + 2n^2)^2 + 4n_{Fe}^2 k_{Fe}^2} \quad (3)$$

where *n*, *k*, and ρ are refraction indices and densities of host material and n_{Fe}, k_{Fe}, and ρ_{Fe} are refraction indices (*37*) and densities of SMFe.

The LMS reflectance spectra were first converted into SSA using Eq. 1. With the reflectance spectra as shown in table S3, we calculated the optical constant *k* of the endmembers and then built a suite of

SSA spectral library by setting the particle size as 5 to 100 μm with an interval of 5 μm. The sparse unmixing algorithm (*38, 39*) was lastly performed to model the SSA spectra of lunar surface using the endmember SSAs. The results are shown in table S4. As shown in Fig. 3 and fig. S5, the residuals of curve fitting in our spectral unmixing analysis are small, and the root mean square values are lower than 4.5×10^{-3}, which is almost equivalent to the calibration uncertainty of the LMS data at around 6% of reflectance values (6% of ~0.07: 4.2×10^{-3}). The elevated ilmenite in D15 and D16 FOV is probably due to the severe shadows (fig. S2) caused by the sampling process.

Deriving water content from the reflectance spectra of lunar surface

SSA between 2.5 and 3.1 μm was calculated from the LMS reflectance spectra using Hapke's model (*21*). The 2.85-μm band was chosen as the water absorption center (Fig. 2 and fig. S1, the black dashed line), which is the same as that used in previous studies to estimate the absolute water content (*9*). The maximum SSA between 2.5 and 3.1 μm was used as the flat line continuum because of the lack of full coverage of the water absorptions from around 2.65 to 4 μm and was used to perform continuum removal for the spectral band at 2.85 μm. The ESPAT value at ~2.85 μm was used to estimate water contents. The ESPAT can be calculated by

$$\mathrm{ESPAT} = \frac{1 - \varpi}{\varpi} \qquad (4)$$

where ϖ is the continuum-removed SSA at 2.85 μm.

Laboratory experiments and simulations have been performed to determine the relationship between ESPAT and water content (*13*). ESPAT at 2.85 μm exhibits a strongly linear correlation with water content with the different slopes of the trend line caused by different particle sizes (*9, 19*). The absolute water content (in parts per million) is estimated as the ESPAT value multiplied by 5000, assuming that the particle size of the regolith is 60 to 80 μm, which is the same as that in (*9, 19*). Previous experiments suggest that the slope between water content (in parts per million) and ESPAT tends to be close to 1900 when the particle size is 1 mm or larger (*9*). Hence, the water content of CE5-Rock and other LMS spectra with rock fragments in the FOV was estimated as the ESPAT value multiplied by 1900 if assuming the particle size of ≥1 mm.

We estimated the detection limit of water content from the ESPAT parameter using the same method in (*9*). The signal-to-noise ratio of the LMS is around 50. We assumed that the noise of the reference band for continuum removal is added to the true signal, and the noise of the 2.85-μm band is subdued from the true signal, which provides the upper limit for an absorption that can be introduced by noises. The ESPAT value was then estimated for this fake OH/H_2O absorption, and thus, the water content was derived as the detection limit. We found that the detection limit of water content for fine regolith (i.e., 60 to 80 μm) is around 30 ppm, and that of the rock (1 mm or bigger) is around 10 ppm. Thus, we chose the detection limit of 30 ppm to be conservative.

SUPPLEMENTARY MATERIALS

REFERENCES AND NOTES

1. B. L. Jolliff, J. J. Gillis, L. A. Haskin, R. L. Korotev, M. A. Wieczorek, Major lunar crustal terranes: Surface expressions and crust-mantle origins. *J. Geophys. Res. Planets* **105**, 4197–4216 (2000).

2. H. Hiesinger, J. Head III, U. Wolf, R. Jaumann, G. Neukum, Ages and stratigraphy of lunar mare basalts in Mare Frigoris and other nearside maria based on crater size-frequency distribution measurements. *J. Geophys. Res. Planets* **115**, E03003 (2010).

3. Y. Qian, L. Xiao, Q. Wang, J. W. Head, R. Yang, Y. Kang, C. H. van der Bogert, H. Hiesinger, X. Lai, G. Wang, Y. Pang, N. Zhang, Y. Yuan, Q. He, J. Huang, J. Zhao, J. Wang, S. Zhao, China's Chang'e-5 landing site: Geology, stratigraphy, and provenance of materials. *Earth Planet. Sci. Lett.* **561**, 116855 (2021).

4. Y. Qian, L. Xiao, S. Y. Zhao, J. N. Zhao, J. Huang, J. Flahaut, M. Martinot, J. W. Head, H. Hiesinger, G. X. Wang, Geology and scientific significance of the Rümker region in northern Oceanus Procellarum: China's Chang'E-5 landing region. *J. Geophys. Res. Planets* **123**, 1407–1430 (2018).

5. Q.-L. Li, Q. Zhou, Y. Liu, Z. Xiao, Y. Lin, J.-H. Li, H.-X. Ma, G.-Q. Tang, S. Guo, X. Tang, J.-Y. Yuan, J. Li, F.-Y. Wu, Z. Ouyang, C. Li, X.-H. Li, Two-billion-year-old volcanism on the Moon from Chang'E-5 basalts. *Nature* **600**, 54–58 (2021).

6. X. Che, A. Nemchin, D. Liu, T. Long, C. Wang, M. D. Norman, K. H. Joy, R. Tartese, J. Head, B. Jolliff, J. F. Snape, C. R. Neal, M. J. Whitehouse, C. Crow, G. Benedix, F. Jourdan, Z. Yang, C. Yang, J. Liu, S. Xie, Z. Bao, R. Fan, D. Li, Z. Li, S. G. Webb, Age and composition of young basalts on the Moon, measured from samples returned by Chang'e-5. *Science* **374**, 887–890 (2021).

7. Z. He, C. Li, R. Xu, G. Lv, L. Yuan, J. Wang, Spectrometers based on acousto-optic tunable filters for in-situ lunar surface measurement. *J. Appl. Remote Sens.* **13**, 027502 (2019).

8. S. Li, R. E. Milliken, An empirical thermal correction model for Moon Mineralogy Mapper data constrained by laboratory spectra and Diviner temperatures. *J. Geophys. Res. Planet* **121**, 2081–2107 (2016).

9. S. Li, R. E. Milliken, Water on the surface of the Moon as seen by the Moon Mineralogy Mapper: Distribution, abundance, and origins. *Sci. Adv.* **3**, e1701471 (2017).

10. M. Ohtake, J. Haruyama, T. Matsunaga, Y. Yokota, T. Morota, C. Honda; LISM team, Performance and scientific objectives of the SELENE (KAGUYA) Multiband Imager. *Earth Planets Space* **60**, 257–264 (2008).

11. H. Otake, M. Ohtake, N. Hirata, in *Lunar and Planetary Science Conference* (2012), p. 1905.

12. Y. Qian, L. Xiao, J. W. Head, C. H. van der Bogert, H. Hiesinger, L. Wilson, Young lunar mare basalts in the Chang'e-5 sample return region, northern Oceanus Procellarum. *Earth Planet. Sci. Lett.* **555**, 116702 (2021).

13. R. E. Milliken, J. F. Mustard, Quantifying absolute water content of minerals using near-infrared reflectance spectroscopy. *J. Geophys. Res. Planets* **110**, E12001 (2005).

14. R. E. Milliken, J. F. Mustard, Estimating the water content of hydrated minerals using reflectance spectroscopy: II. Effects of particle size. *Icarus* **189**, 574–588 (2007).

15. B. M. French, G. Heiken, D. Vaniman, *Lunar Sourcebook: A User's Guide to the Moon* (CUP Archive, 1991).

16. C. Li, H. Hu, M. F. Yang, Z. Y. Pei, Q. Zhou, X. Ren, B. Liu, D. Liu, X. Zeng, G. Zhang, H. Zhang, J. Liu, Q. Wang, X. Deng, C. Xiao, Y. Yao, D. Xue, W. Zuo, Y. Su, W. Wen, Z. Ouyang, Characteristics of the lunar samples returned by Chang'E-5 Mission. *Natl. Sci. Rev.* nwab188 (2021).

17. Z. Wang, Y. Wu, D. T. Blewett, E. A. Cloutis, Y. Zheng, J. Chen, Submicroscopic metallic iron in lunar soils estimated from the in situ spectra of the Chang'E-3 mission. *Geophys. Res. Lett.* **44**, 3485–3492 (2017).

18. Y. Liu, Y. Guan, Y. Zhang, G. R. Rossman, J. M. Eiler, L. A. Taylor, Direct measurement of hydroxyl in the lunar regolith and the origin of lunar surface water. *Nat. Geosci.* **5**, 779–782 (2012).

19. R. E. Milliken, S. Li, Remote detection of widespread indigenous water in lunar pyroclastic deposits. *Nat. Geosci.* **10**, 561–565 (2017).

20. A. Stephant, F. Robert, The negligible chondritic contribution in the lunar soils water. *Proc. Natl. Acad. Sci.* **111**, 15007–15012 (2014).

21. B. Hapke, Bidirectional reflectance spectroscopy: 1. Theory. *J. Geophys. Res. Solid Earth* **86**, 3039–3054 (1981).

22. S. A. Li, L. Li, Radiative transfer modeling for quantifying lunar surface minerals, particle size, and submicroscopic metallic Fe. *J. Geophys. Res. Planet* **116**, E09001 (2011).

23. P. D. Spudis, in *The Encyclopedia of Volcanoes*, H. Sigurdsson, B. Houghton, S. R. McNutt, H. Rymer, J. Stix, Eds. (Elsevier, 2015), pp. 689–700.

24. A. E. Saal, E. H. Hauri, J. A. Van Orman, M. J. Rutherford, Hydrogen isotopes in lunar volcanic glasses and melt inclusions reveal a carbonaceous chondrite heritage. *Science* **340**, 1317–1320 (2013).

25. R. Klima, J. Cahill, J. Hagerty, D. Lawrence, Remote detection of magmatic water in Bullialdus Crater on the Moon. *Nat. Geosci.* **6**, 737–741 (2013).

26. S. Bhattacharya, A. Dagar, S. Saran, M. Chauhan, P. Chauhan, Endogenic water on the Moon associated with non-mare silicic volcanism: Implications for hydrated lunar interior. *Curr. Sci.* **105**, 685–691 (2013).

27. A. E. Saal, E. H. Hauri, M. L. Cascio, J. A. van Orman, M. C. Rutherford, R. F. Cooper, Volatile content of lunar volcanic glasses and the presence of water in the Moon's interior. *Nature* **454**, 192–195 (2008).

28. S. Li, G. J. Taylor, R. Lentz, D. H. Needham, L. Gaddis, T. Shea, in *Lunar and Planetary Science Conference* (2021), p. 2508.

29. B. Jolliff, M. Robinson, S. Ravi, Origin and Evolution of the Moon's Procellarum KREEP Terrane. *Bull. Am. Astronom. Soc.* **53**, 294 (2021).

30. H. Lin, S. Li, Y. Lin, Y. Liu, Y. Wei, W. Yang, Y. Yang, S. Hu, X. Wu, R. Xu, C. Li, Z. He, Thermal modeling of the lunar regolith at the Chang'E-4 landing site. *Geophys. Res. Lett.* **48**, e2020GL091687 (2021).

31. J. F. Mustard, C. M. Pieters, Photometric phase functions of common geologic minerals and applications to quantitative analysis of mineral mixture reflectance spectra. *J. Geophys. Res. Solid Earth* **94**, 13619–13634 (1989).

32. Y. Yang, S. Li, R. E. Milliken, H. Zhang, K. Robertson, T. Hiroi, Phase functions of typical lunar surface minerals derived for the hapke model and implications for visible to near-infrared spectral unmixing. *J. Geophys. Res. Planets* **124**, 31–60 (2019).

33. C. M. Pieters, D. Stankevich, Y. G. Shkuratov, L. Taylor, Statistical analysis of the links among lunar mare soil mineralogy, chemistry, and reflectance spectra. *Icarus* **155**, 285–298 (2002).

34. L. Taylor, A. Patchen, D. Taylor, J. Chambers, D. McKay, X-ray digital imaging petrography of lunar mare soils: Modal analyses of minerals and glasses. *Icarus* **124**, 500–512 (1996).

35. N. Keshava, J. F. Mustard, Spectral unmixing. *IEEE Sig. Process. Mag.* **19**, 44–57 (2002).

36. Y. Shkuratov, Y. Grynko, Light scattering by media composed of semitransparent particles of different shapes in ray optics approximation: Consequences for spectroscopy, photometry, and polarimetry of planetary regoliths. *Icarus* **173**, 16–28 (2005).

37. M. R. Querry, *Optical Constants* (Missouri Univ-Kansas City, 1985).

38. M.-D. Iordache, J. M. Bioucas-Dias, A. Plaza, Sparse unmixing of hyperspectral data. *IEEE Trans. Geosci. Remote Sens.* **49**, 2014–2039 (2011).

39. H. Lin, J. F. Mustard, X. Zhang, A methodology for quantitative analysis of hydrated minerals on Mars with large endmember library using CRISM near-infrared data. *Planet. Space Sci.* **165**, 124–136 (2019).